Zhou *et al. EURASIP Journal on Advances in Signal Processing* (2021) 2021:68
https://doi.org/10.1186/s13634-021-00781-z

EURASIP Journal on Advances in Signal Processing

RESEARCH Open Access

Aerial intelligent reflecting surface-enhanced cell-free massive MIMO for high-mobility communication: joint Doppler compensation and power optimization

Tao Zhou, Kui Xu, Wei Xie*, Zhexian Shen, Chen Wei, Jie Liu and Linpu Sun

*Correspondence:
edifier77@163.com
Army Engineering University of PLA, Nanjing, China

Abstract

Intelligent reflecting surfaces (IRSs) are considered one of the core technologies in sixth-generation (6G) mobile communication. In this paper, we investigate an aerial IRS (AIRS)-enhanced cell-free (CF) massive multiple-input-multiple-output (MIMO)system where multiple APs serve a high-speed mobile user simultaneously. The mobility of the user leads to fast time-varying and nonnegligible Doppler frequency offsets (DFOs), which cause a serious threat to link performance. To overcome the influence of the Doppler effect and reduce the energy consumption of the system, we propose a Doppler compensation and transmission method by using the AIRS. Specifically, we divide the AIRS reflection phase shift vector into two parts: one part is used for Doppler compensation, and the other is used for transmission. First, we propose an angle-sensing algorithm to obtain the user angle in each coherent time (CT) and use it to design a Doppler compensation vector. Then, we propose an angle information-aided transmission strategy to design the transmission reflecting vector, the beamforming vector, and the power allocation coefficient of each AP to minimize the transmission power of all APs at a required achievable rate. The simulation results show that we can significantly reduce the total transmission power by using the proposed method.

Keywords: Aerial intelligent reflecting surface, Cell-free massive MIMO, Doppler compensation, Transmission optimization

1 Introduction

With the deployment of fifth-generation (5G) mobile communication, the industry has started extensive research on sixth-generation (6G) communication. In addition to satisfying higher performance requirements in communication, we must address the rising costs and energy consumption in 6G. As one of the core technologies of 6G, intelligent reflecting surfaces (IRSs) can effectively solve the cost and energy consumption problems in wireless communication [1, 2], so they have attracted increasing attention in recent years.

© The Author(s). 2021 **Open Access** This article is licensed under a Creative Commons Attribution 4.0 International License, which permits use, sharing, adaptation, distribution and reproduction in any medium or format, as long as you give appropriate credit to the original author(s) and the source, provide a link to the Creative Commons licence, and indicate if changes were made. The images or other third party material in this article are included in the article's Creative Commons licence, unless indicated otherwise in a credit line to the material. If material is not included in the article's Creative Commons licence and your intended use is not permitted by statutory regulation or exceeds the permitted use, you will need to obtain permission directly from the copyright holder. To view a copy of this licence, visit http://creativecommons.org/licenses/by/4.0/.

IRSs are composed of an intelligent controller and a reflecting array. They are also called large intelligent surfaces (LISs) [3, 4] or reconfigurable intelligent surfaces (RISs) [5–7]. The intelligent controller is connected to the transmitter to control the reflecting array. This array is composed of abundant low-cost elements, each of which is a sub-wavelength structure that can independently control the phase of the reflected signal. An intelligent controller can jointly control each element to adjust the phase of the reflected signal, so that the reflected signal can be coherently superimposed in the desired direction, which is called passive beamforming [8]. Compared with traditional relays, IRSs are not equipped with signal sensing elements, so they cannot receive and process the signal before reflecting it. An IRS only passively reflects the incident signal. Thus, the IRS offers advantages in energy consumption and cost [9, 10].

Massive MIMO is now widely used in 5G cellular networks [11, 12]. The deployment of large-scale array antennas at BSs can satisfy the users' needs for high-capacity and high-speed service, but there are problems such as intercell interference and capacity limits. To solve these problems, cell-free (CF) massive MIMO has been proposed as a new architecture. In a CF massive MIMO system, multiple distributed access points (APs) simultaneously serve several users in the coverage area under the control of a central processing unit (CPU) [13–15]. Specifically, the CPU controls all APs to jointly serve the users by scheduling the resources to achieve coherent transmission [16, 17]. CF massive MIMO eliminates the cell boundary and solves the problems of intercell interference and capacity capping in cellular networks and is considered a core architecture of 6G communication.

1.1 Motivations and contributions

The existing IRS application scenarios mainly focus on traditional cellular networks such as single-input-single-output (SISO) communication systems [18], multiple-input-single-output (MISO) communication systems [19, 20], MIMO communication systems [21, 22] and multicell MIMO communication systems [23]. However, there are few studies on IRS-aided CF massive MIMO systems. As the core technologies of next-generation wireless communication, the combination of IRSs and CF massive MIMO is an inevitable trend. This application can fully utilize IRS features such as low cost and flexible deployment while enhancing the spectrum efficiency, energy efficiency, and area coverage of future wireless communications. In addition, only a few studies have considered IRS-aided high-speed mobile scenes [24, 25]. High mobility decreases the coherent time (CT) and causes a Doppler shift, which leads to intercarrier interference (ICI) [26]. Therefore, the communication performance is greatly degraded.

Motivated by these reasons, this paper studies an IRS-enhanced downlink CF massive MIMO system, where multiple APs simultaneously serve a high-speed mobile user through an aerial IRS (AIRS) [27, 28]. The mobility of the user causes the Doppler frequency offset (DFO), which cannot be ignored. To overcome the influence of the Doppler effect and reduce the total transmit power of APs, we propose an AIRS-based joint Doppler compensation and transmission optimization strategy. We propose to use the AIRS to perform Doppler compensation instead of using APs; thus, the complexity of beamforming at each AP is reduced. By jointly designing the AIRS Doppler compensation vector, beamforming vector and power allocation vector at each AP, and AIRS reflecting vector, we can minimize the total transmit power.

1.2 Organizations

In Section 2, we summarize the method and contributions of this paper. In Section 3, we research the system model and characterize the Doppler channel model. Then, in Section 4, we research the AIRS-assisted Doppler compensation strategy. We analyse how to use the AIRS to compensate for the Doppler frequency offset (DFO) and propose an angle-sensing strategy to obtain the user's angle according to the estimated cascade channel in each CT. Based on the user angle information, we construct the Doppler compensation vector at the AIRS to compensate for the DFO. In Section 5, we propose an angle information-aided downlink transmission method to minimize the transmission power of APs. In Section 6, we analyse the effectiveness of the proposed algorithm by simulation in a real scene. Section 7 summarizes this paper.

1.3 Notations

We use a slant letter for a constant B and bold italic small letters to denote a vector $\boldsymbol{p}$. Matrices are represented by bold capital letters. The argument of complex number B is denoted by $\arg(B)$. For vector $\boldsymbol{p}$, we use $\arg(\boldsymbol{p})$ to express its corresponding argument vector. $\mathrm{diag}(\boldsymbol{p})$ denotes a diagonal matrix whose diagonal element is the corresponding element in $\boldsymbol{p}$; $\mathbf{A}^{\mathrm{H}}$ denotes the conjugate transpose matrix of $\mathbf{A}$; $\mathbf{A}^{\mathrm{T}}$ is the transpose matrix of $\mathbf{A}$; $\odot$ is the Hadamard product.

2 Method

To perform Doppler compensation and optimize the total transmit power, we divide the design of the AIRS reflection phase shift coefficient into two parts: one part for the Doppler compensation and the other part for the transmission optimization.

To compensate for the DFO, we study the characteristics of the Doppler channel and find that the DFO exists in the channel between users and AIRS and is associated with the angle of arrival (AoA). If the AoA information is obtained, we can calculate the DFO and design the AIRS reflection phase shift coefficient to compensate for it. Therefore, we propose an angle-sensing algorithm to obtain the angle information of the user from the estimated cascade channel and construct a Doppler compensation vector. Then, we propose an angle information-aided transmission optimization strategy to optimize the transmission power of all APs during each CT.

3 System model and channel characteristics

In this section, we will introduce the system and study the channel model. As shown in Fig. 1, in a CF massive MIMO system, K APs provide services for a mobile user under the control of a CPU at the same time. The CPU and AP are connected via a backhaul link. The communication quality of the direct path between the user and the APs is poor due to the shielding of the tall building. To fully use air-to-ground resources and reduce the additional AP deployment overhead, we use an AIRS to assist the communication. The AIRS is equivalent to a passive relay that reflects the signals from APs to the user. The AIRS is placed on a UAV[1]. The CPU controls the AIRS by communicating with the smart controller of the AIRS. The speed of the user is v. The DFO is caused by high-speed movement. To improve the quality of service (QoS) of the user, we must compensate for the DFO.

[1] In this paper, we assume that AIRS is placed on a UAV parallel to the ground. The location of the UAV is fixed and is known by the CPU.

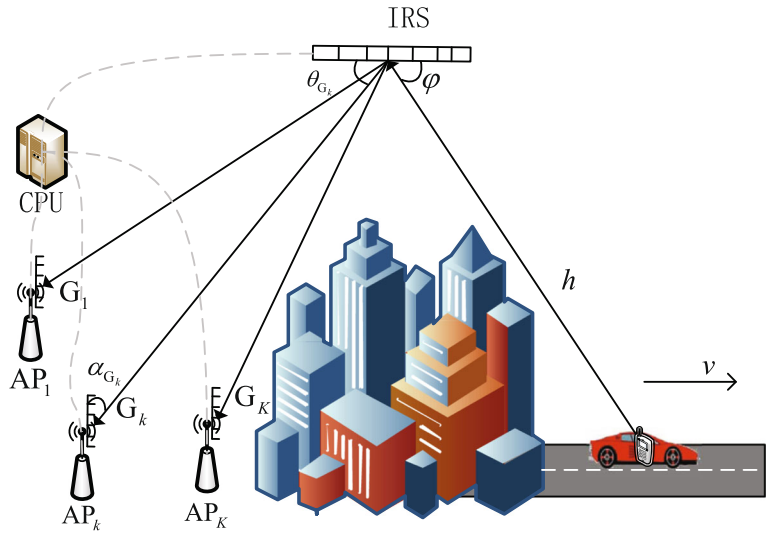

Fig. 1 System model

We research a time-division duplex (TDD) system. Due to the reciprocity, we can obtain the downlink channel state information (CSI) by uplink channel estimation. Assume that the AIRS is equipped with N reflection elements. We consider the uniform linear array (ULA) channel model[2]. $\boldsymbol{h}$ denotes the channels from the user to the AIRS. $G_k, k = 1..., K$ denotes the channels from the AIRS to the k-th AP. We assume that the APs and AIRS are fixed during communication, so there is DFO in channel $\boldsymbol{h}$.

Channel $\mathbf{G}_k$ in the n-th CT can be expressed as

$$\mathbf{G}_{k,n} = \sum_{l=1}^{L_1} e^{j\phi_n} \chi_l \beta_{\mathbf{G}_{k,l,n}} \mathbf{a}_M \left(\alpha_{k,l,n}\right) \mathbf{a}_N^{\mathrm{H}} \left(\theta_{k,l,n}\right) \tag{1}$$

According to the multi-path fading channel model in [25, 29–31], the uplink channel from the mobile user to AIRS is modelled as

$$\boldsymbol{h}_n = \sum_{l=1}^{L_2} e^{j\left(\phi_n + \phi_{f_{D_{l,n}}}\right)} \chi_l \beta_{\boldsymbol{h}_{l,n}} \mathbf{a}_N \left(\varphi_{l,n}\right) \odot \boldsymbol{b}_{l,n} \tag{2}$$

We assume that channels $\mathbf{G}_k, k = 1..., K$ consist of L_1 paths, and channel $\boldsymbol{h}$ consists of L_2 paths. In addition, $l = 1$ is the line-of-sight (LoS) path of each channel. χ_l is the weight parameter of each path. The AIRS is in the air; thus, the LoS path is stronger than the non-line-of-sight (NLoS) paths in this ground-to-air scenario [27, 28, 32]. We set χ_l as follows:

$$\chi_l = \begin{cases} \sqrt{\frac{\kappa}{\kappa+1}} & l = 1 \\ \sqrt{\frac{\kappa}{(\kappa+1)(L-1)}} & l \geq 2 \end{cases} \tag{3}$$

where κ is the Rice factor, and L is the number of paths corresponding to the channel. $\beta_l \in \mathcal{N}\left(0, {\delta_l}^2\right)$ denotes the complex gain; ${\delta_l}^2$ is the path loss of the corresponding path; ϕ_n is the phase of the carrier frequency; $\phi_n = 2\pi f_c n T$, T is the length of each CT; $\phi_{f_{D_{l,n}}}$ is the absolute phase shift that arises from the Doppler effect; $\phi_{f_{D_{l,n}}} = 2\pi f_{D_{l,n}} n T$. $f_{D_{l,n}}$ is the

[2]To simplify the channel model, the ULA form is considered in this paper, but it is feasible to extend to the uniform planar array (UPA).

frequency shift arising from the Doppler effect; $f_{D_{l,n}} = \frac{c_u}{\lambda}\cos\left(\varphi_{l,n}\right)$; $\varphi_{l,n}$ is the AoA of the l-th path for channel $\boldsymbol{h}$; $\alpha_{k,l,n}$ and $\theta_{k,l,n}$ are the AoA and AoD of the l-th path for channel $\mathbf{G}_k$; $\mathbf{a}_M(\theta)$ is the steering vector, which can be written as

$$\mathbf{a}_M(\theta)=\left[1, e^{j2\pi\frac{d}{\lambda}\cos(\theta)}, ..., e^{j2\pi\frac{d}{\lambda}(M-1)\cos(\theta)}\right]^{\mathrm{T}} \tag{4}$$

where d is the antenna or element spacing, and λ is the wavelength. Because of the element spacing and Doppler effect, the relative DFO $\mathbf{b}_{l,n}$ occurs when the signal reaches the array elements of the AIRS, and we can write $\boldsymbol{b}_{l,n}$ as

$$\boldsymbol{b}_{l,n} = \left[1, e^{j2\pi\frac{dc_u}{\lambda c}\cos^2\left(\varphi_{l,n}\right)}, ..., e^{j2\pi\frac{dc_u}{\lambda c}(N-1)\cos^2\left(\varphi_{l,n}\right)}\right]^{\mathrm{T}} \tag{5}$$

where c is the propagation velocity of the electromagnetic wave.

4 AIRS-assisted angle sensing and Doppler compensation

4.1 AIRS-assisted Doppler compensation

First, we explain how to use the AIRS to conduct Doppler compensation. The received signal at the user in the n-th CT is

$$\begin{aligned} y_n &= \boldsymbol{h}_n^{\mathrm{H}}\mathbf{V}\mathbf{G}_{1,n}^{\mathrm{H}}\boldsymbol{\zeta}_1\sqrt{P\eta_1}x + \boldsymbol{h}_n^{\mathrm{H}}\mathbf{V}\mathbf{G}_{2,n}^{\mathrm{H}}\boldsymbol{\zeta}_2\sqrt{P\eta_2}x +, \\ &\ldots, + \boldsymbol{h}_n^{\mathrm{H}}\mathbf{V}\mathbf{G}_{K,n}^{\mathrm{H}}\boldsymbol{\zeta}_K\sqrt{P\eta_K}x + \varepsilon \\ &= \sum_{k=1}^{K}\boldsymbol{h}_n^{\mathrm{H}}\mathbf{V}\mathbf{G}_{k,n}^{\mathrm{H}}\boldsymbol{\zeta}_k\sqrt{P\eta_k}x + \varepsilon \end{aligned} \tag{6}$$

Here, x is the information-bearing signal [27]. $\boldsymbol{\zeta}_k$ is the beamforming vector of the k-th AP; ε is additive white Gaussian noise (AWGN); η_k is the power allocation coefficient of the k-th AP (AP_k) and satisfies $\sum_{k=1}^{K}\eta_k = 1$; P is the total transmit power of all Aps; $\mathbf{V}$ is the reflection coefficient matrix; $\mathbf{V} = \mathrm{diag}(\boldsymbol{\nu})$, $\boldsymbol{\nu} = \left[e^{j\varsigma_1}, e^{j\varsigma_2}, ..., e^{j\varsigma_N}\right]^{\mathrm{T}}$ is the reflection coefficient vector; ς_n is the phase shift coefficient of the n-th element at the AIRS.

As discussed earlier, the LoS path is much stronger than the NLoS paths; since the channels are dominated by the former in ground-to-air communication, we focus on the LoS path. For the convenience of analysis, we simplify channels $\mathbf{G}_{k,n}$ and $\boldsymbol{h}_n$ as

$$\mathbf{G}_{k,n} = e^{j\phi_n}\beta_{\mathbf{G}_{k,n}}\mathbf{a}_M\left(\alpha_{k,n}\right)\mathbf{a}_N^{\mathrm{H}}\left(\theta_{k,n}\right) \tag{7}$$

$$\boldsymbol{h}_n = e^{j\left(\phi_n+\phi_{f_{D_n}}\right)}\beta_{\boldsymbol{h}_n}\mathbf{a}_N\left(\varphi_n\right)\odot\boldsymbol{b}_n \tag{8}$$

Equations (7) and (8) indicate that the DFO only exists in channel $\boldsymbol{h}_n$. Specifically, the absolute DFO $\phi_{f_{D_n}}$ and relative DFO $\boldsymbol{b}_n$ are in channel $\boldsymbol{h}_n$. According to (5), the elements of $\boldsymbol{b}_{l,n}$ are approximately 1 because the user's speed c_u is much slower than the speed of light c. Therefore, we can mainly compensate the absolute DFO $\phi_{f_{D_n}}$. However, for completeness, we compensate for both $\phi_{f_{D_n}}$ and $\boldsymbol{b}_{l,n}$. The main idea is to compensate for the DFO in the LoS path of $\boldsymbol{h}_n$ by setting the reflection coefficients of the AIRS elements.

Inserting (7) and (8) into (6), we obtain

$$\begin{aligned} y_n &= \sum_{k=1}^{K} \boldsymbol{h}_n^{\mathrm{H}} \mathbf{V} \mathbf{G}_{k,n}^{\mathrm{H}} \boldsymbol{\zeta}_k \sqrt{P\eta_k} x + \varepsilon \\ &= \boldsymbol{h}_n^{\mathrm{H}} \mathbf{V} \sum_{k=1}^{K} \mathbf{G}_{k,n}^{\mathrm{H}} \boldsymbol{\zeta}_k \sqrt{P\eta_k} x + \varepsilon \\ &= \boldsymbol{h}_n^{\mathrm{H}} \boldsymbol{\Psi} \boldsymbol{\Xi} \sum_{k=1}^{K} \mathbf{G}_{k,n}^{\mathrm{H}} \boldsymbol{\zeta}_k \sqrt{P\eta_k} x + \varepsilon \end{aligned} \tag{9}$$

Here, we divide the reflection coefficient matrix $\mathbf{V}$ into two parts: one part for the Doppler compensation and the other for the transmission. We define $\mathbf{V} = \boldsymbol{\Psi}\boldsymbol{\Xi}$, where $\boldsymbol{\Psi}$ is a Doppler compensation matrix; Ξ is a reflection matrix to assist the transmission, and $\boldsymbol{\Xi} = \mathrm{diag}\left(e^{j\omega_1}, ..., e^{j\omega_n}\right)$; ω_n is the reflection phase shift for transmission. We use Ψ to compensate for the DFO and Ξ to optimize the AIRS-aided transmission. To this end, we must obtain f_{D_n}. Then, we can calculate $\phi_{f_{D_n}}$. Note that $f_{D_{l,n}} = \frac{c_u}{\lambda}\cos\left(\varphi_{l,n}\right)$. In this paper, we consider that the user's speed is constant and known by the CPU. If we obtain φ_n in each CT, the absolute DFO can be calculated. Then, we set Ψ as

$$\Psi = e^{j\phi_{f_D}} \mathrm{diag}\left(1, e^{j2\pi \frac{dv}{\lambda c}\cos^2(\varphi)}, ..., e^{j2\pi \frac{dv}{\lambda c}(N-1)\cos^2(\varphi)}\right) \tag{10}$$

which compensates for the DFO.

The key idea is to obtain the AoA of the LoS path in channel $\boldsymbol{h}$ in each CT and set $\boldsymbol{\Psi}$ as (10) to compensate for the DFO for the LoS path. Following compensation, we can use the angle information to find an optimal $\boldsymbol{\Xi}$ for the downlink transmission. Therefore, the acquisition of user angle φ becomes the key work in this paper.

4.2 Angle-sensing strategy

In this subsection, we introduce how to use the AIRS to perceive the user angle φ. We find that the traditional AoA estimation method in a massive MIMO system is not applicable to this system. Then, we analyse the angle-domain characteristic of the AIRS reflecting channel, turn the angle estimation into an optimization problem, and propose an angle-sensing strategy to estimate φ.

First, we review the traditional methods of AoA estimation and discuss the feasibility of the direct application of AoA estimation in AIRS-assisted systems. In massive MIMO systems, we can estimate the AoA of the channel by discrete Fourier transform (DFT). Due to the angle expansion and sparsity of the channel, the energy of the channel is concentrated at only a few points following the DFT application.

Suppose that a channel from a single antenna user to an AP is $\boldsymbol{h}_0$. $\boldsymbol{h}_0$ only consists of one path and can be expressed as $\boldsymbol{h}_0 = \beta \mathbf{a}_{M_0}(\psi)$. We define $\boldsymbol{\Gamma}_M$ as the DFT matrix.

$$\Gamma_M = \begin{bmatrix} 1 & 1 & \cdots & 1 \\ 1 & e^{-j2\pi\frac{1}{M}} & \cdots & e^{-j2\pi\frac{1}{M}(M-1)} \\ \cdots & \cdots & \cdots & \cdots \\ 1 & e^{-j2\pi\frac{1}{M}(M-1)} & \cdots & e^{-j2\pi\frac{1}{M}(M-1)^2} \end{bmatrix} \tag{11}$$

The DFT of $\boldsymbol{h}_0$ can be expressed as

$$\begin{aligned}\boldsymbol{s} &= \Gamma_{M_0} h_0 \\ &= \beta \begin{bmatrix} 1 & 1 & \dots & 1 \\ 1 & e^{-j2\pi\frac{1}{M_0}} & \dots & e^{-j2\pi\frac{1}{M_0}(M_0-1)} \\ \dots & \dots & \dots & \dots \\ 1 & e^{-j2\pi\frac{1}{M_0}(M_0-1)} & \dots & e^{-j2\pi\frac{1}{M_0}(M_0-1)^2} \end{bmatrix} \\ &\quad \begin{bmatrix} 1 \\ e^{j2\pi\frac{d}{\lambda}\cos(\psi)} \\ \dots \\ e^{j2\pi\frac{d}{\lambda}(M_0-1)\cos(\psi)} \end{bmatrix}\end{aligned} \tag{12}$$

The k-th element in $|\boldsymbol{s}|$ is

$$[\,|\boldsymbol{s}|]_k = \left|\beta e^{j2\pi\frac{M_0-1}{2}\left(\frac{d}{\lambda}\cos(\psi)-\frac{k-1}{M_0}\right)} \frac{\sin\left(2\pi\frac{M_0}{2}\left(\frac{d}{\lambda}\cos(\psi)-\frac{k-1}{M_0}\right)\right)}{\sin\left(2\pi\frac{1}{2}\left(\frac{d}{\lambda}\cos(\psi)-\frac{k-1}{M_0}\right)\right)}\right| \tag{13}$$

Equation (13) indicates that $\boldsymbol{s}_k$ takes the maximum value only if $\frac{d}{\lambda}\cos(\psi) - \frac{k-1}{M_0} = 0$.

In Fig. 2, we present an example for the DFT of $\boldsymbol{h}_0$. We set the true AoA as $\psi = 25°, 45°$ and 75°. The AP is equipped with 30 antennas, and the antenna spacing is 0.5. For different angles of ψ, the maximum value of $|\boldsymbol{h}_0|$ corresponds to different beam indices in the x-label. In other words, we can distinguish different AOAs by the DFT method due to the difference in x-label.

Then, we consider how to obtain the user's angle φ in an AIRS-aided system. First, we apply the DFT method directly to obtain φ. In this case, the channel from the user to the

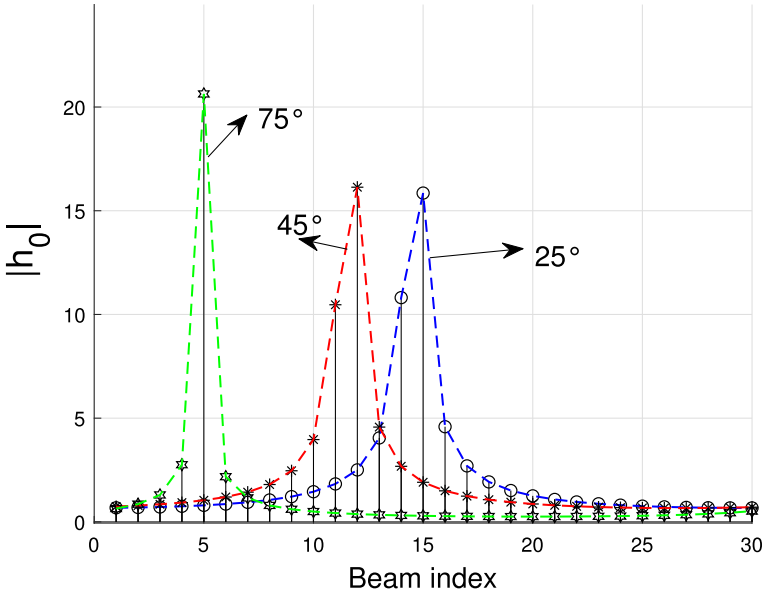

Fig. 2 DFT of channel $\boldsymbol{h}_0$

k-th AP can be written as

$$\begin{aligned}
&\mathbf{H}_k = \mathbf{G}_k \mathbf{V} \boldsymbol{h} \\
&= \mathbf{G}_k \mathrm{diag}(\boldsymbol{h}) \boldsymbol{v} \\
&= \\
&\beta e^{2\pi \cos(\varphi)} \begin{bmatrix} \sum_{n=1}^{N} e^{j\varsigma_n + j2\pi \frac{d}{\lambda}(n-1)(\cos(\varphi)-\cos(\theta))} \\ \sum_{n=1}^{N} e^{j\varsigma_n + j2\pi \frac{d}{\lambda}\left[\cos(\alpha)+(n-1)(\cos(\varphi)-\cos(\theta))\right]} \\ \cdots \\ \sum_{n=1}^{N} e^{j\varsigma_n + j2\pi \frac{d}{\lambda}\left[(M-1)\cos(\alpha)+(n-1)(\cos(\varphi)-\cos(\theta))\right]} \end{bmatrix}
\end{aligned} \tag{14}$$

where β is the product of complex gain in channels $\mathbf{G}_k$ and $\boldsymbol{h}$. Here, we set $\omega_n = 0, n = 1, ..., N$ to study the influence of different user angles φ on the DFT. We set $\theta = 30°, \alpha = 60°$, and $\varphi = [0°, 20°, 30°, 40°, 50°, 60°]$, $M = 20$ and $\frac{d}{\lambda} = 0.5$. As shown in Fig. 3, following the DFT application, identical beam indices correspond to the maximum values of different values of φ. Hence, we cannot use the conventional DFT method to estimate φ because we cannot distinguish different angles in the x-label. Thus, we must find another method to obtain φ. We define $\mathbf{H}_k{}^{\mathrm{DFT}} = \Gamma_M \mathbf{H}_k$. The s-th element of $|\mathrm{H}_k{}^{\mathrm{DFT}}|$ can be expressed as

$$\begin{aligned}
&\left[|\mathbf{H}_k{}^{\mathrm{DFT}}|\right]_s \\
&= \left[|\Gamma_M \mathbf{H}_k|\right]_s \\
&= |\beta e^{j2\pi \cos(\varphi)} BC|
\end{aligned} \tag{15}$$

where

$$B = \sum_{n=1}^{N} e^{j\varsigma_n + j2\pi\left[\frac{d}{\lambda}(n-1)(\cos(\varphi)-\cos(\theta))\right]} \tag{16}$$

$$C = e^{j\pi(M-1)X} \frac{\sin(\pi M X)}{\sin(\pi X)} \tag{17}$$

and

$$X = \frac{d}{\lambda}\cos(\alpha) - \frac{s-1}{M} \tag{18}$$

Equation (15) - (18) reveal that after the DFT transformation, the maximum value of $|\mathbf{H}_k{}^{\mathrm{DFT}}|$ is obtained if and only if $X = 0$. X is only related to the angle α, not to angles φ or θ. Here, α is the AoA of channel $\mathbf{G}_k$. When φ is set to different values, channel $\mathbf{G}_k$ is invariant; thus, α and θ are constants. Therefore, identical beam indices correspond to the maximum value of $|\mathbf{H}_k{}^{\mathrm{DFT}}|$ in different φ after the DFT implementation. In this time, channel $\boldsymbol{h}$ becomes a coefficient of C. Different values of φ only change B, which is the amplitude of $|\mathbf{H}_k{}^{\mathrm{DFT}}|$. Therefore, we cannot use the DFT method to directly obtain φ in an IRS-aided communication system.

In this paper, we propose an angle-sensing algorithm to estimate φ. In the AIRS-aided CF massive MIMO system, the positions of all APs are usually fixed. The AIRS is controlled by the CPU, so the location of the AIRS is also known. We can assume that the angle information of channel $\mathbf{G}_k, k = 1, ..., K$ is known. This assumption is reasonable and has been used in many IRS-related studies. From (16), we can find the maximum value of B if we find a set of optimal AIRS reflection coefficients $\varsigma_n, n = 1, ..., N$. When B reaches

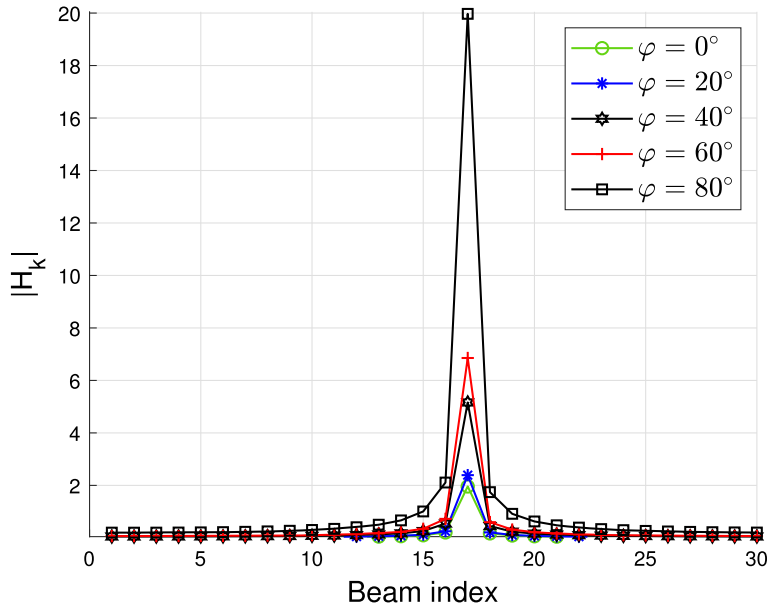

Fig. 3 DFT of channel $\mathbf{H}_k$

the maximum value, $|\mathbf{H}_k{}^{\mathrm{DFT}}|$ also reaches the maximum value. In this case, the following equation holds:

$$\begin{aligned} &j\varsigma_n + j2\pi\left[\tfrac{d}{\lambda}(n-1)(\cos(\varphi)-\cos(\theta))\right] = j\Omega \\ &n = 1,...,N \end{aligned} \tag{19}$$

where $\Omega \in [0, 2\pi)$ is an alignment angle. To obtain the maximum value, all additions of B should have the same phase $e^{j\Omega}$. For ease of argument, we set $\Omega = 0$. When we find ς_n to maximize B, we have the following equation:

$$\varsigma_n = 2\pi\left[\frac{d}{\lambda}(n-1)(\cos(\theta)-\cos(\varphi))\right] \tag{20}$$

Then, we can obtain φ. To find the optimal $\varsigma_n, n = 1,...,N$, we construct the optimization problem as

$$\begin{aligned} &\mathrm{P1}: \\ &\max_{\varsigma_n} \sum_{n=1}^{N} e^{j\varsigma_n + j2\pi\left[\frac{d}{\lambda}(n-1)(\cos(\varphi)-\cos(\theta))\right]} e^{j\pi(M-1)X} \\ &\quad \times \tfrac{\sin(\pi MX)}{\sin(\pi X)} e^{j2\pi\cos(\varphi)} \\ &\quad s.t.\ \ \varsigma_n \in [0, 2\pi), n = 1,...,N; \\ &\qquad X = \tfrac{d}{\lambda}\cos(\alpha) - \tfrac{s-1}{M}; \end{aligned} \tag{21}$$

From (19), we find that the optimal set of ς_n has the form of an arithmetic sequence, and $\varsigma_0 = 0$. Thus, we set $\varsigma_n = (n-1)\vartheta, \vartheta \in \left[-2\pi\tfrac{d}{\lambda}, 2\pi\tfrac{d}{\lambda}\right]$, where $X = 0$ is the reference point. Then, (P1) can be rewritten as

$$\begin{aligned} &\mathrm{P2}: \\ &\max_{\vartheta} \sum_{n=1}^{N} e^{j(n-1)\vartheta + j2\pi\left[\frac{d}{\lambda}(n-1)(\cos(\varphi)-\cos(\theta))\right]} \\ &\quad \mathrm{s.t.}\vartheta \in \left[-2\pi\tfrac{d}{\lambda}, 2\pi\tfrac{d}{\lambda}\right] \end{aligned} \tag{22}$$

Note that

$$\begin{aligned}&\sum_{n=1}^{N} e^{j(n-1)\vartheta + j2\pi\left[\frac{d}{\lambda}(n-1)(\cos(\varphi)-\cos(\theta))\right]}\\&= \sum_{n=1}^{N} e^{j(n-1)\left[\vartheta + 2\pi\frac{d}{\lambda}(\cos(\varphi)-\cos(\theta))\right]}\\&= e^{j2\pi\frac{N-1}{2}}\frac{\sin(N\pi\chi)}{\sin(\pi\chi)}\end{aligned} \tag{23}$$

where $\chi = \left[\vartheta + 2\pi\frac{d}{\lambda}(\cos(\varphi) - \cos(\theta))\right]$. When $\chi = 0$, (P2) can be solved, leading to

$$\vartheta_{opt} = 2\pi\frac{d}{\lambda}\left[\cos(\theta) - \cos(\varphi)\right] \tag{24}$$

Here, the key idea is to find $\vartheta \in \Upsilon$, $\Upsilon = \left[-2\pi\frac{d}{\lambda}, 2\pi\frac{d}{\lambda}\right]$ to solve (P2). Then, we can obtain φ by (24). To find ϑ, we perform a one-dimensional search in Υ with an appropriate search accuracy Δ[3].

We do not truly adjust the reflection coefficient ς_n at the AIRS but simply match the angle at the CPU. Specifically, we first estimate the cascade channel $\mathbf{Ht}_k$, $\mathbf{Ht}_k = \mathbf{G}_k\mathrm{diag}(\boldsymbol{h})$. Then, we use a sensing vector $\boldsymbol{\nu}_p$ to solve (P2) and obtain φ. Here, $\boldsymbol{\nu}_p$ is defined as

$$\boldsymbol{\nu}_p = \left[1, e^{j\vartheta}, ..., e^{j(N-1)\vartheta}\right]^{\mathrm{T}} \tag{25}$$

The specific algorithm implementation is summarized in Algorithm 1. When φ is obtained, we can construct $\boldsymbol{\Psi}$ by (10) to compensate for the DFO.

Algorithm 1 Angle-sensing strategy (A1).

Input: The estimated cascade channel $\mathbf{Ht}_k$, search accuracy Δ, α_k, θ_k

Output: The sensed angle of $\widetilde{\varphi}$

1. Define the search space as $\Upsilon = \left[-2\pi\frac{d}{\lambda} : \Delta : 2\pi\frac{d}{\lambda}\right]$. Select beam index $i = \left\lfloor M\frac{d}{\lambda}\cos(\theta) + 1\right\rfloor$ as a reference beam index.

2.For each $\vartheta \in \Upsilon$:

Constructing angle sensing vector $\boldsymbol{\nu}_p$ by (25).

Calculate $\boldsymbol{q}_k = \mathbf{Ht}_k\boldsymbol{\nu}_p$.

Perform DFT for $\boldsymbol{q}_k$, obtain $|\boldsymbol{q}_k{}^{\mathrm{DFT}}|_{id}$

end

3. Find the ϑ_{opt} which maximizes $|\boldsymbol{q}_{k\mathrm{DFT}}|_i$.

4. Obtain the estimated $\widetilde{\varphi}$ by (24)

5 Angle-information-aided downlink transmission strategy

After the DFO compensation, we use the angle information to optimize the downlink transmission. In this section, we propose an angle information-aided strategy for downlink transmission. For a required achievable rate R_0, our goal is to minimize the total transmission power of all APs P by jointly designing the beamforming vectors $\boldsymbol{\xi} = [\xi_1, \xi_2, ..., \xi_K]$, power allocation coefficient $\boldsymbol{\eta} = [\eta_1, \eta_2, ..., \eta_K]$, and reflection matrix for transmission $\boldsymbol{\Xi}$, $\boldsymbol{\Xi} = \mathrm{diag}\left(e^{j\omega_1}, ..., e^{j\omega_n}\right)$.

[3]Our goal is to find an optimal value ϑ from a given interval Υ. Since the range of Υ is small, a simple one-dimensional search is appropriate. Of course, other search algorithms can be used to reduce the complexity.

According to (9), the objective function is constructed as follows:

$$\begin{aligned}
&\text{P3}\\
&\min_{\boldsymbol{\xi},\boldsymbol{\eta},\boldsymbol{\Xi}} \quad P\\
&\text{s.t. } \log_2\left(1+P\frac{\left|\sum_{k=1}^{K}\boldsymbol{h}^{\mathrm{H}}\mathbf{V}\mathbf{G}_k^{\mathrm{H}}\boldsymbol{\xi}_k\sqrt{\eta_k}\right|^2}{\varepsilon^2}\right)\geq R_0;\\
&\sum_{k=1}^{K}\eta_k=1;\\
&\left\|\boldsymbol{\xi}_k\right\|=1, k=1,...,K;\\
&\mathbf{V}=\boldsymbol{\Psi}\boldsymbol{\Xi};\\
&\boldsymbol{\Xi}=\mathrm{diag}\left(e^{j\omega_1},e^{j\omega_2},...,e^{j\omega_N}\right);\\
&\omega_n\in[0,2\pi), n=1,...,N;
\end{aligned} \tag{26}$$

In (26), under a given achievable rate constraint to minimize P, we must maximize $\frac{\left|\sum_{k=1}^{K}\boldsymbol{h}^{\mathrm{H}}\mathbf{V}\mathbf{G}_k^{\mathrm{H}}\boldsymbol{\xi}_k\sqrt{\eta_k}\right|^2}{\varepsilon^2}$. Problem (P3) can be simplified to[4]

$$\begin{aligned}
&\max_{\boldsymbol{\xi},\boldsymbol{\eta},\boldsymbol{\Xi}}\left|\sum_{k=1}^{K}\boldsymbol{h}^{\mathrm{H}}\boldsymbol{\Psi}\boldsymbol{\Xi}\mathbf{G}_k^{\mathrm{H}}\boldsymbol{\xi}_k\sqrt{\eta_k}\right|^2\\
&\text{s.t. }\sum_{k=1}^{K}\eta_k=1;\\
&\left\|\boldsymbol{\xi}_k\right\|=1, k=1,...,K;\\
&\boldsymbol{\Xi}=\mathrm{diag}\left(e^{j\omega_1},e^{j\omega_2},...,e^{j\omega_N}\right);\\
&\omega_n\in[0,2\pi), n=1,...,N;
\end{aligned} \tag{27}$$

First, we optimize the beamforming vectors $[\boldsymbol{\xi}_1,\boldsymbol{\xi}_2,...,\boldsymbol{\xi}_K]$. As discussed earlier, the locations of each AP and the AIRS are known by the CPU, so α_k and θ_k are determined. To maximize the transmission performance, we should optimize the beamforming vector $\boldsymbol{\xi}_k$ to make the beam of AP_k point to the AIRS [27]. Thus, the optimal beamforming vector for AP_k is

$$\boldsymbol{\xi}_k{}^{opt}=\frac{1}{\sqrt{M}}\mathbf{a}_M(\alpha_k) \tag{28}$$

Then, we optimize $\boldsymbol{\Xi}$. After the DFO compensation, $\boldsymbol{b}_n$ and ϕ_{f_D} are compensated. Then, we have

$$\begin{aligned}
&\sum_{k=1}^{K}h^{\mathrm{H}}\Psi\,\Xi\mathbf{G}_k^{\mathrm{H}}\boldsymbol{\xi}_k\sqrt{\eta_k}\\
&=\sum_{k=1}^{K}\beta_k\sqrt{\eta_k}\mathbf{a}_N^{\mathrm{H}}(\varphi)\,\boldsymbol{\Xi}\,\mathbf{a}_N(\theta_k)
\end{aligned} \tag{29}$$

where β_k is the product of complex gain in channels $\mathbf{G}_k$ and $\boldsymbol{h}$. Note that

$$\begin{aligned}
&\sum_{k=1}^{K}\mathbf{a}_N^{\mathrm{H}}(\varphi)\,\boldsymbol{\Xi}\sqrt{\eta_k}\mathbf{a}_N(\theta_k)\\
&=\mathbf{a}_N^{\mathrm{H}}(\varphi)\,\boldsymbol{\Xi}\Big[\sqrt{\eta_1}\mathbf{a}_N(\theta_1)+\sqrt{\eta_2}\mathbf{a}_N(\theta_2)+\\
&...+\sqrt{\eta_K}\mathbf{a}_N(\theta_K)\Big]\\
&=\mathbf{u}\boldsymbol{\Xi}\mathbf{w}
\end{aligned} \tag{30}$$

[4] If the channel energy is fixed, the transmit power P is minimal when we take an equal sign for the achievable rate constraint. Under a given achievable rate constraint, the channel energy should be maximized to reduce the transmission power P.

where $\mathbf{w} = \sqrt{\eta_1}\mathbf{a}_N(\theta_1) + \sqrt{\eta_2}\mathbf{a}_N(\theta_2) + ... + \sqrt{\eta_K}\mathbf{a}_N(\theta_K)$ and $\mathbf{u} = \mathbf{a}_N^{\mathrm{H}}(\varphi)$. To maximize $\boldsymbol{u}\boldsymbol{\Xi}\mathbf{w}$, $\boldsymbol{\Xi}$ should be designed to align the phases of $\boldsymbol{u}$ and $\mathbf{w}$. The optimal ω_n is

$$\omega_n^{opt} = e^{j(\Omega - \arg([\boldsymbol{u}]_n[\mathbf{w}]_n))}, n = 1, \ldots, N \tag{31}$$

Ω is the alignment phase of a reference. Another method to optimize $\boldsymbol{\Xi}$ is the local reflection coefficient design. We select the AP_c that is closest to the user and design $\boldsymbol{\Xi}$ to maximize $\mathbf{a}_N^{\mathrm{H}}(\varphi)\boldsymbol{\Xi}\mathbf{a}_N(\theta_c)$; the optimal ω_n is

$$\omega_n^{opt'} = e^{j\frac{2\pi d}{\lambda}(n-1)[\cos(\varphi)-\cos(\theta_c))]}. \tag{32}$$

This type of local phase shift design is relatively simple, but the signal from other APs is not considered, so the performance is degraded. When $\boldsymbol{\Xi}$ is determined, the equivalent channel $\mathbf{H}_k$ from AP_k to the user is determined. We can allocate power according to the gain of the current equivalent channel $\mathbf{H}_k$ from AP_k, and the optimal $\boldsymbol{\eta}$ is

$$\eta_k^{opt} = \frac{\|\mathbf{H}_k\|^2}{\sum_{k=1}^{K}\|\mathbf{H}_k\|^2}, k = 1, \ldots, K. \tag{33}$$

The algorithm implementation is detailed in Algorithm 2.

Algorithm 2 Angle-information-aided transmission optimization algorithm (A2).

Input: The estimated cascade channel $\mathbf{Ht}_k$, $\alpha_k, \theta_k, k = 1, ..., K$, sensing angle of $\widetilde{\varphi}$, required achievable rate R_0 and DFO compensation vector Ψ.

Output: The optimal $\boldsymbol{\xi}$,$\boldsymbol{\eta}$,$\boldsymbol{\Xi}$, and optimized total transmission power P.

1. Initialize $\boldsymbol{\xi}$ randomly. Set $\boldsymbol{\eta}$ =[$1/K, 1/K, ..., 1/K$].

2. For $k = 1 \rightarrow K$

Obtain ${\boldsymbol{\xi}_k}^{opt}, k = 1, ..., K$ by (28).

For $n = 1 \rightarrow N$

Obtain ω_n^{opt} by (31)

end

Construct vector $\boldsymbol{\Xi}$ =[$e^{j\omega_1}, ..., e^{j\omega_n}$].

Obtain $\mathbf{H}_k$ by (14) and obtain the optimal $\boldsymbol{\eta}$ by (33).

end

4. Calculate P by using the expression of the achievable rate in (26).

6 Results and discussion

In this section, we simulate a real scene and analyse the effectiveness of these proposed methods. In Fig. 4, the number of APs is set as $K = 3$ (the CPU is omitted for brevity). The number of antennas at each AP is set as $M = 10$, and the AIRS is equipped with $N = 100$ elements. The user is on the x-axis and moves towards the positive direction. We set the user's coordinates as $(x, 0, 0), x \in [120, 200]$. The user's speed is $v = 20$ m/s. The specific settings are shown in Table 1.

The path loss β is set according to the 3GPP Urban Microcell model in [33] and can be expressed as

$$\beta(D) = -30.5 - 36.7\lg(D) + o \tag{34}$$

where D is the distance and $o \sim \mathcal{N}\left(0, 4^2\right)$ denotes shadow fading.

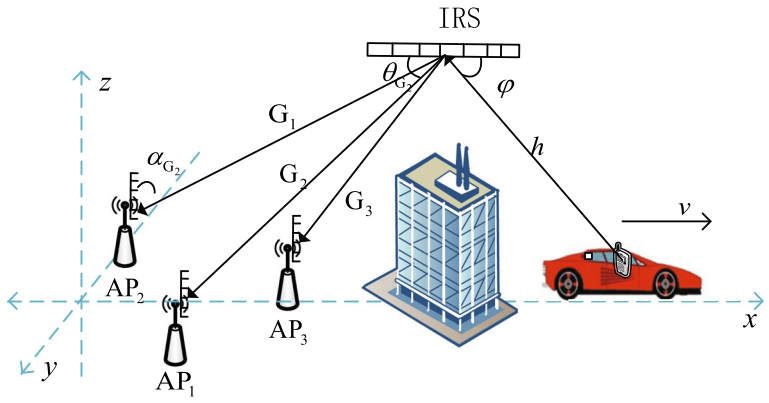

Fig. 4 Simulation scene

Now, we analyse the performance of the angle-sensing algorithm.

First, we assume that the CSI is perfectly known and study the performance of the angle-sensing method. We randomly set the user's coordinates in [120, 200] and use Algorithm 1 to sense φ under different search accuracies Δ. We perform 1000 randomized trials and average them. We use the mean error (ME) to evaluate the performance of the angle sensing method, which can be written as follows:

$$\mathrm{ME} = \frac{\sum_{k=1}^{K} |\varphi - \widehat{\varphi}_k|}{K}. \tag{35}$$

where φ_k is the estimated value of φ at the k-th AP. As shown in Fig. 5, the proposed algorithm has high estimation accuracy. When Δ increases, the error of angle sensing increases, but the error is within a few degrees. When $\Delta = 0.01$, the sensed angle is very nearly identical to the real angle of the user.

Then, in Fig. 6, we study the impact of the channel estimation error on the performance of the angle-sensing method. We use the least-squares (LS) method proposed in [34] to

Table 1 Simulation settings

Parameter	Value
Bandwidth	1 MHz
Number of APs K	3
Number of AP antennas M	10
Number of paths for each channel L	10
Number of AIRS elements N	100
the noise power	−96 dBm
Rice factor κ	100
Coordinates of AP_1(m)	(50,25,0)
Coordinates of AP_2(m)	(80,30,0)
Coordinates of AP_3(m)	(80,-20 ,0)
Coordinates of AIRS(m)	(120,0,60)
User speed	20 m/s
Velocity of electromagnetic waves c	3×10^8 m/s
Wavelength λ	0.15 m
Length of one CT T	3 ms
Antenna or element spacing d	0.5λ

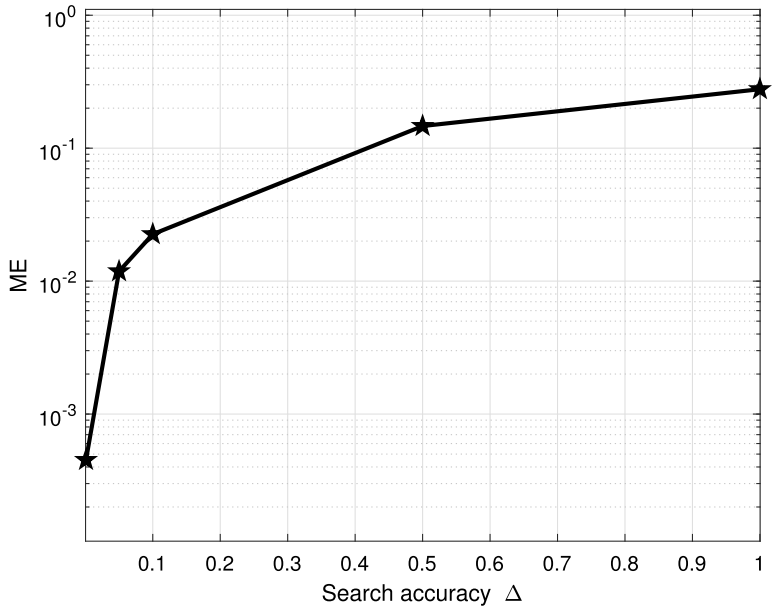

Fig. 5 Performance analysis with perfect CSI

estimate that cascaded channel $\mathbf{Ht}_k, k = 1, ..., K$[5]. The user sends a pilot to each AP, and each AP estimates the cascaded channel using the LS method. The length of the pilot is set to $\tau = 4$, and the number of subframes is set to N. After the channel estimation, all APs send the estimated channel $\mathbf{Ht}_k, k = 1, ..., K$ to the CPU, and the CPU performs angle sensing by Algorithm 1. Then, the CPU obtains K estimated angles $\widehat{\varphi}_k, k = 1, ..., K$. We use the average signal-to-noise ratio (SNR) to measure the performance of the proposed algorithm. The definition of SNR is similar to [35]. Define SNR $= \frac{\beta_k P_t \tau}{\sigma^2}$, where β_k is the pathloss of the cascaded channel $\mathbf{Ht}_k$, P_t is the transmitting power of the user.

As Fig. 6 shows, under different values of search accuracy Δ, the estimation error of the user's angle decreases with an increased SNR because the channel estimation error decreases if we increase the SNR. Thus, the angle estimation becomes more accurate. However, with increasing SNR, the angle estimation error tends to be constant in the high-SNR cases because in the high-SNR cases, the channel estimation is sufficiently accurate. At this time, the main factor that limits the angle estimation is the search accuracy Δ. We also find that under a given SNR, we can obtain a more precise angle of the user by using a smaller search accuracy Δ. In fact, using the smaller search accuracy Δ will lead to higher computational complexity. In addition, we find that the search accuracy Δ has the greatest impact on the estimation performance. Even when SNR = -10 dB, the estimation error can be reduced to less than 0.1 if $\Delta \leq 0.1$. Therefore, we can choose an appropriate Δ to weigh the relationship between computational complexity and SNR.

Then, we analyse the performance of the proposed Algorithm 2. In the first CT, the user's coordinate is (130,0,0). In this case, we mainly analyse the performance of the proposed transmission method, so we assume that the CSI and angle information are perfectly known by the CPU.

[5]CSI is important for IRS-aided communications. In this paper, we mainly consider the Doppler compensation and transmission strategy for AIRS-aided cell-free massive MIMO systems, and channel estimation is not our primary concern. Actually, the acquisition of CSI remains challenging, especially for AIRS-aided cell-free systems. Therefore, a more efficient channel estimation method will be our future work.

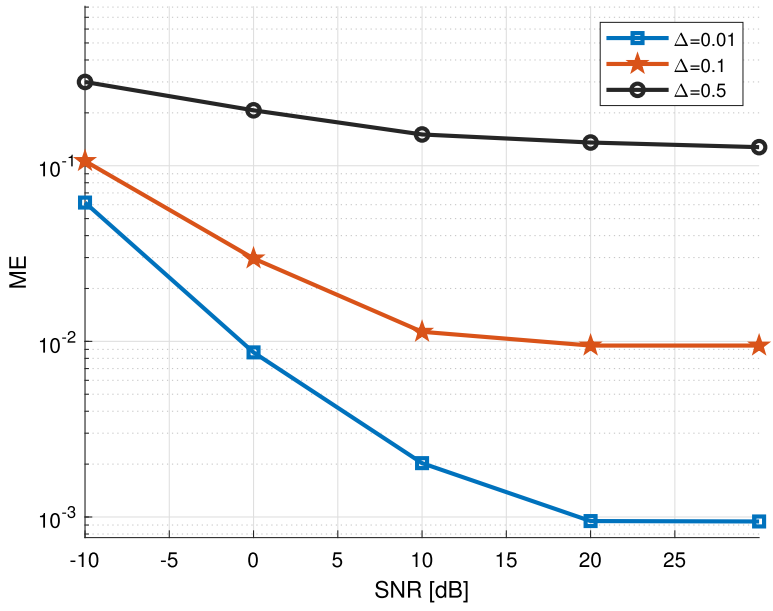

Fig. 6 Performance analysis with imperfect CSI

In Fig. 7, we compare the performance in five different settings to verify the performance of the proposed Algorithm 2.

1) **Random phase (RP) with equal power allocation (EPA)**: In this case, we randomly set each element of $\boldsymbol{\Xi}$ and allocate equal power to each AP.

2) **Global phase (GP) optimization with EPA**: We use the proposed AIRS phase optimization method in (31) to optimize $\boldsymbol{\Xi}$ and allocate equal power to each AP.

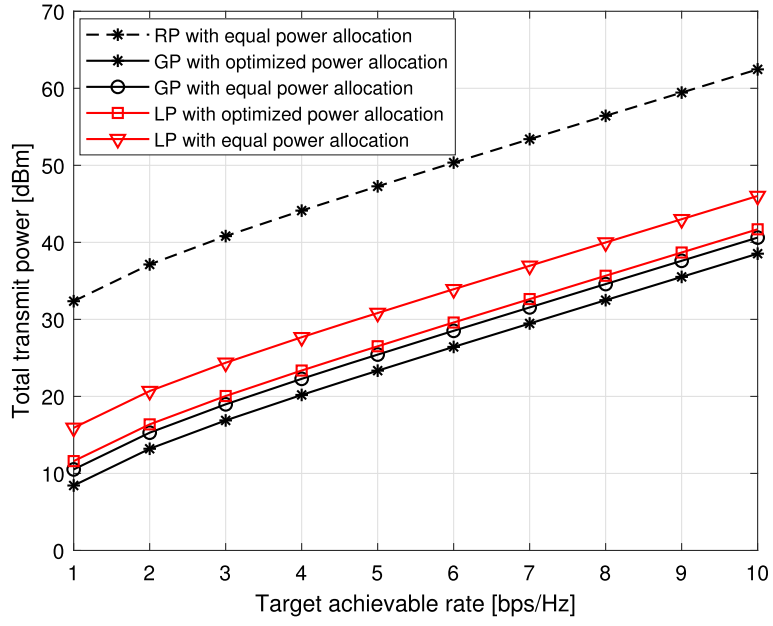

Fig. 7 Performance comparison under different settings

3) **GP with optimized power allocation (OPA)**: We use the proposed Algorithm 2 to optimize both $\boldsymbol{\Xi}$ and power allocation vector $\boldsymbol{\eta}$.

4) **Local phase (LP) optimization with EPA**: We use the proposed AIRS phase optimization method in (32) to optimize $\boldsymbol{\Xi}$ and allocate equal power to each AP.

5) **LP with optimized power allocation (OPA)**: We use the proposed AIRS phase optimization method in (32) to optimize $\boldsymbol{\Xi}$ and use (33) to obtain the power allocation vector $\boldsymbol{\eta}$.

Figure 7 shows that at a given target achievable rate, compared with the RP with the equal power allocation method, the proposed transmission strategy can significantly reduce the total transmit power. The GP method performs better than the LP method, which implies that the design of the AIRS reflection phase shift coefficients with multiple AP synergisms can provide better performance. Moreover, compared with the equal power allocation method, the total transmission power can be further reduced by using the power allocation method. Therefore, the proposed algorithm shows good performance in reducing energy consumption.

In Fig. 8, we study the influence of the number of AIRS elements N on the power-saving performance. The required achievable rate is $R_0 = 5$ bps/Hz. We compare the proposed GP and LP methods under different AIRS N. As Fig. 8 shows, the proposed GP method shows better performance than the LP method. In addition, the total transmission power can be reduced by increasing the number of AIRS elements N. Therefore, we can equip more elements at the AIRS to reduce energy consumption. However, it may be challenging to equip the AIRS with many elements because they increase the element cost. In addition, the AIRS is deployed on a UAV, and the payload on the UAV is limited. These factors should be considered in actual deployment.

7 Conclusion

In this paper, we study an AIRS-enhanced CF massive MIMO system where the AIRS is used to assist communication between multiple APs and a high-speed mobile user.

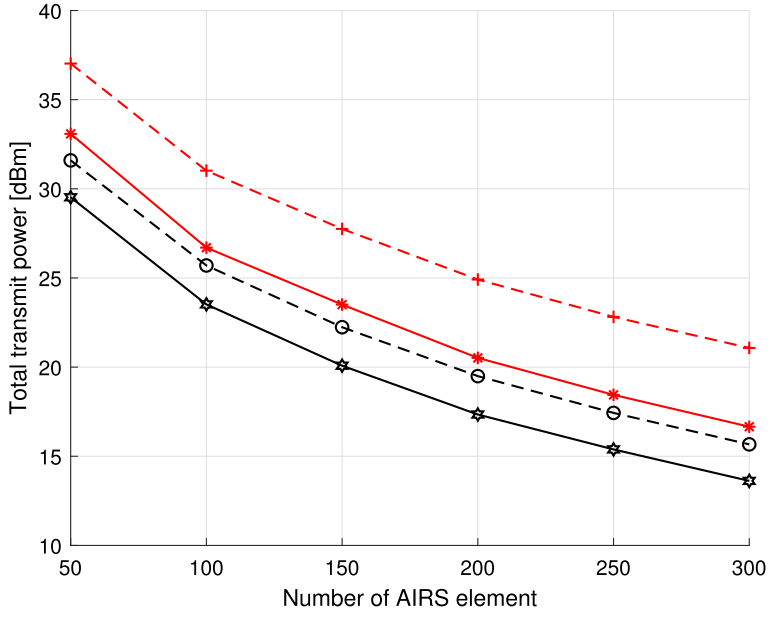

Fig. 8 Effect of the AIRS element N

To eliminate the influence of the Doppler effect, we use the AIRS to perform Doppler compensation and aid in communication. Specifically, we divide the design of the air reflection phase shift coefficient into two parts: a Doppler compensation vector and a reflecting optimization vector. For Doppler compensation, we propose an angle-sensing algorithm to obtain the user's angle in each CT to design the Doppler compensation vector at the AIRS. To minimize the transmission power, we propose an angle information-aided transmission algorithm to jointly design the reflecting optimization vector at the AIRS, power allocation vectors, and beamforming vectors at the APs. The simulation results show that by using the proposed angle-sensing method, we can obtain accurate angle information of the user. The total transmission power can be significantly reduced by the proposed transmission strategy. The results of this paper prompt further study. First, in this paper, we mainly studied the Doppler compensation and transmission strategy of this system and did not fully consider the channel estimation strategy. The LS method in this paper requires considerable training. Therefore, we must explore more efficient channel estimation methods. Second, by improving the angle-sensing algorithm, we can use IRS to locate users to integrate communication and location. We plan to explore these aspects in our future work.

Abbreviations

IRS: Intelligent reflecting surface; AIRS: Aerial intelligent reflecting surface; DFO: Doppler frequency offset; CF massive MIMO: Cell-free massive multiple-input-multiple-output; CT :Coherent time; LIS: Large intelligent surfaces; DF: Decode and forward; AP: Access point; CPU: Central processing unit; SISO: Single-input-single-output; MISO: Multiple-input-single-output; ICI: Intercarrier interference; UAV: Unmanned aerial vehicle; QoS: Quality of service; TDD: Time-division duplex; CSI: Channel state information; ULA: Uniform linear array; LoS: line-of-sight; NLoS: Non-line-of-sight; AoA: Angle of arrival; AWGN: Additive white Gaussian noise; DFT: Discrete Fourier transform;

Acknowledgements

The authors would like to thank the editor and the anonymous reviewers for their helpful comments and suggestions.

Authors' contributions

All authors made contributions in the discussions, analyses, and implementation of the proposed solution. TZ also contributed in writing the manuscript. All authors read and approved the final manuscript.

Funding

This work was supported in part by the Natural Science Foundation of Jiangsu Province under Grant BK20181335; the National Natural Science Foundation of China under Grant 62071485, Grant 61901519, Grant 61771486, and Grant 61671472; the Basic Research Project of Jiangsu Province under Grant BK20192002; and the Natural Science Foundation of Jiangsu Province under Grant BK20201334.

Availability of data and materials

The datasets used and/or analysed during the current study are available from the corresponding author on reasonable request.

Declarations

Competing interests

The authors declare that they have no competing interests.

Received: 18 May 2021 Accepted: 26 July 2021
Published online: 14 August 2021

References

1. Q. Wu, R. Zhang, Towards smart and reconfigurable environment: intelligent reflecting surface aided wireless network. IEEE Commun. Mag. **58**(1), 106–112 (2020)
2. M. D. Renzo, et al., Smart radio environments empowered by recon- figurable AI meta-surfaces: An idea whose time has come. J. Wirel. Commun. Netw. **2019**(1), 129 (2019)
3. S. Hu, K. Chitti, F. Rusek, O. Edfors, in *2018 IEEE 29th Annual International Symposium on Personal, Indoor and Mobile Radio Communications (PIMRC)*, User assignment with distributed large intelligent surface (LIS) systems, (2018), pp. 1–6
4. Y. Han, W. Tang, S. Jin, C. Wen, X. Ma, Large Intelligent Surface-Assisted Wireless Communication Exploiting Statistical CSI. IEEE Trans. Veh. Technol. **68**(8), 8238–8242 (2019)

5. E. Basar, M. Di Renzo, J. De Rosny, M. Debbah, M. Alouini, R. Zhang, Wireless communications through reconfigurable intelligent surfaces. IEEE Access. **7**, 116753–116773 (2019)
6. M. Di Renzo, A. Zappone, M. Debbah, M. -S. Alouini, C. Yuen, J. de Rosny, S. Tretyakov, Smart radio environments empowered by reconfigurable intelligent surfaces: how it works, state of research, and the road ahead. IEEE J. Sel. Areas Commun. **38**(11), 2450–2525 (2020)
7. W. Tang, et al., Wireless communications with reconfigurable intelligent surface: path loss modeling and experimental measurement. IEEE Trans. Wirel. Commun. **20**(1), 421–439 (2021)
8. Q. Wu, R. Zhang, in *2018 IEEE Global Communications Conference (GLOBECOM)*, Intelligent reflecting surface enhanced wireless network: joint active and passive beamforming design, (2018), pp. 1–6
9. M. Di Renzo, et al., Reconfigurable intelligent surfaces vs. relaying: differences, similarities, and performance comparison. IEEE Open J. Commun. Soc. **1**, 798–807 (2020)
10. S. Hu, F. Rusek, O. Edfors, Beyond massive MIMO: the potential of data transmission with large intelligent surfaces. IEEE Trans. Signal Process. **66**(10), 2746–2758 (2018)
11. E. G. Larsson, O. Edfors, F. Tufvesson, T. L. Marzetta, Massive MIMO for next generation wireless systems. IEEE Commun. Mag. **52**(2), 186–195 (2014)
12. J. G. Andrews, et al., What Will 5G Be? IEEE J. Sel. Areas Commun. **32**(6), 1065–1082 (2014)
13. H. Q. Ngo, A. Ashikhmin, H. Yang, E. G. Larsson, T. L. Marzetta, Cell-free massive MIMO versus small cells. IEEE Trans. Wirel. Commun. **16**(3), 1834–1850 (2017)
14. E. Nayebi, A. Ashikhmin, T. L. Marzetta, H. Yang, B. D. Rao, Precoding and power optimization in cell-free massive MIMO systems. IEEE Trans. Wirel. Commun. **16**(7), 4445–4459 (2017)
15. H. Q. Ngo, A. Ashikhmin, H. Yang, E. G. Larsson, T. L. Marzetta, Cell-free massive MIMO versus small cells. IEEE Trans. Wirel. Commun. **16**(3), 1834–1850 (2017)
16. S. Shamai, B. M. Zaidel, in *IEEE VTS 53rd Vehicular Technology Conference, Spring 2001. Proceedings (Cat. No. 01CH37202)*, Enhancing the cellular downlink capacity via co-processing at the transmitting end, vol. 3, (2001), pp. 1745–1749
17. E. Björnson, L. Sanguinetti, Making Cell-Free Massive MIMO Competitive With MMSE Processing and Centralized Implementation. IEEE Trans. Wirel. Commun. **19**(1), 77–90 (2020)
18. E. Björnson, Ö. Özdogan, E. G. Larsson, Intelligent reflecting surface versus decode-and-forward: how large surfaces are needed to beat relaying? IEEE Wirel. Commun. Lett. **9**(2), 244–248 (2020)
19. Q. Wu, R. Zhang, Intelligent reflecting surface enhanced wireless network via joint active and passive beamforming. IEEE Trans. Wirel. Commun. **18**(11), 5394–5409 (2019)
20. X. Yu, D. Xu, R. Schober, in *2019 IEEE/CIC International Conference on Communications in China (ICCC)*, MISO wireless communication systems via intelligent reflecting surfaces: (Invited Paper), (2019), pp. 735–740
21. S. Zhang, R. Zhang, Capacity Characterization for Intelligent Reflecting Surface Aided MIMO Communication. IEEE J. Sel. Areas Commun. **38**(8), 1823–1838 (2020)
22. S. Zhang, R. Zhang, in *2020 IEEE International Symposium on Information Theory (ISIT)*, On the Capacity of Intelligent Reflecting Surface Aided MIMO Communication, (2020), pp. 2977–2982
23. C. Pan, et al., Multicell MIMO communications relying on intelligent reflecting surfaces. IEEE Trans. Wirel. Commun. **19**(8), 5218–5233 (2020)
24. E. Basar, I. F. Akyildiz, Reconfigurable intelligent surfaces for doppler effect and multipath fading mitigation. arXiv preprint arXiv:1912.04080 (2019)
25. Z. Huang, B. Zheng, R. Zhang, Transforming fading channel from fast to slow: IRS-assisted high-mobility communication. arXiv preprint arXiv:2011.03147 (2019)
26. K. Xu, Z. Shen, Y. Wang, X. Xia, Location-aided mMIMO channel tracking and hybrid beamforming for high-speed railway communications: an angle-domain approach. IEEE Syst. J. **14**(1), 93–104 (2020)
27. H. Lu, Y. Zeng, S. Jin, R. Zhang, in *2020 IEEE International Conference on Communications Workshops (ICC Workshops)*, Enabling panoramic full-angle reflection via aerial intelligent reflecting surface, (2020), pp. 1–6
28. H. Lu, Y. Zeng, S. Jin, R. Zhang, Aerial intelligent reflecting surface: joint placement and passive beamforming design with 3D beam flattening. IEEE Trans. Wirel. Commun. **20**(7), 4128–4143 (2021)
29. Z. Shen, K. Xu, X. Xia, W. Xie, D. Zhang, Spatial sparsity based secure transmission strategy for massive MIMO systems against simultaneous jamming and eavesdropping. IEEE Trans. Inf. Forensics Secur. **15**, 3760–3774 (2020)
30. H. Yin, D. Gesbert, M. Filippou, Y. Liu, A coordinated approach to channel estimation in large-scale multiple-antenna systems. IEEE J. Sel. Areas Commun. **31**(2), 264–273 (2013)
31. J. -A. Tsai, R. M. Buehrer, B. D. Woerner, in *IEEE 55th Vehicular Technology Conference. VTC Spring 2002 (Cat. No.02CH37367)*, The impact of AOA energy distribution on the spatial fading correlation of linear antenna array, vol. 2, (2002), pp. 933–937
32. Y. Zeng, Q. Wu, R. Zhang, Accessing from the sky: a tutorial on UAV communications for 5G and beyond. Proc. IEEE. **107**(12), 2327–2375 (2019)
33. E. Björnson, L. Sanguinetti, Making cell-free massive MIMO competitive with MMSE processing and centralized implementation. IEEE Trans. Wirel. Commun. **19**(1), 77–90 (2020)
34. J. Chen, Y. Liang, H. Cheng, W. Yu, Channel estimation for reconfigurable intelligent surface aided multi-user MIMO systems. arXiv preprint arXiv:1912.03619 (2020)
35. D. Mishra, H. Johansson, in *2019 IEEE International Conference on Acoustics, Speech and Signal Processing*, Channel estimation and low-complexity beamforming design for passive intelligent surface assisted MISO wireless energy transfer, (2019), pp. 4659–4663

Publisher's Note

Springer Nature remains neutral with regard to jurisdictional claims in published maps and institutional affiliations.